Cite this article
Philia J, Widayat W and Sulardjaka S
Amorphous adsorbent from geothermal solid waste for methylene blue removal. *Journal of Environmental Engineering and Science*,
https://doi.org/10.1680/jenes.21.00082

Research Article
Paper 2100082
Received 21/12/2021; Accepted 03/08/2022

Journal of Environmental Engineering and Science

ice Publishing

Amorphous adsorbent from geothermal solid waste for methylene blue removal

1 **John Philia** ST, MT
PhD student, Department of Mechanical Engineering, Diponegoro University, Semarang, Indonesia (Orcid:0000-0003-3032-1705)

2 **Widayat Widayat** ST, MT, IPM
Professor, Department of Chemical Engineering, Diponegoro University, Semarang, Indonesia (Orcid:0000-0003-1906-2378)
(corresponding author: widayat@live.undip.ac.id)

3 **Sulardjaka Sulardjaka** ST, MT, IPU
Lecturer, Department of Mechanical Engineering, Diponegoro University, Semarang, Indonesia (Orcid:0000-0001-8273-0469)



Organic compounds such as dyes and heavy metal ions are common pollutants in waste water that have become a global problem. Adsorption has proven to be a successful technique in removing organic species such as methylene blue (MB). Geothermal solid waste has the potential to be used as an adsorbent due to its silica content. The silica compound in geothermal waste has the potential to be developed as porous material. Aluminium hydroxide and geothermal solid waste were added to the aqueous alkali (sodium hydroxide (NaOH)) in a continuous stirred-tank reactor, which resulted in an amorphous mesoporous material of the natrolite phase. The performance of the geoadsorbent was evaluated through the removal of various concentrations of MB, and isotherm adsorption models were used to evaluate the data. The adsorption mechanisms of MB removal by the geoadsorbent as shown by Fourier transform infrared spectra are electrostatic attraction and hydrogen-bond formation. The geoadsorbent can remove MB up to 84.449%, in which the adsorption is highly dependent on the initial concentration of MB. The Langmuir isotherm model provides the most accurate representation of MB adsorption as a result of the physical process, with a correlation coefficient of 0.971.

Keywords: adsorption/methylene blue

Notation

C_0	initial methylene blue concentration
C_e	methylene blue remaining equilibrium concentration
E	methylene blue removal percentage
K_F	Freundlich constant related to adsorption capacity
K_L	Langmuir constant related to adsorption capacity
K_T	Temkin constant related to adsorption capacity
m	adsorbent mass
q_e	equilibrium concentration of the adsorbate
q_m	practical limiting adsorption capacity
V	solution volume

Introduction

The large amount of dye waste water generated in industrial processes is one of the leading worldwide environmental issues that must be resolved to ensure sustainable production. Methylene blue (MB; $C_{16}H_{18}ClN_3S{\cdot}H_2O$) is a cationic dye that has been widely used in industries (Jawad and Abdulhameed, 2020; Nakhli *et al*., 2020; Shindhal *et al*., 2021). Essential issues of MB pollution are the harmful effect on human health, aesthetic damage to waters and aquatic ecosystem disruption. MB is toxic to humans and (at a certain amount) can cause vomiting, headache, eye/skin irritation, high blood pressure, shortness of breath and rapid heartbeat. It is also considered a major threat to humans because of chromosomal breakage, aneuploidy and generated micronuclei in human cells due to its carcinogenic and mutagenic properties (Jalali *et al*., 2019; Mahamad *et al*., 2015). Limited light penetration to water caused by MB pollution reduces dissolved oxygen levels and photosynthesis rate, which affect the aquatic ecosystem. The MB compound in water is very hazardous to soil microorganisms, plant germination and growth (Lellis *et al*., 2019; Rehman *et al*., 2018).

Adsorption is considered the most efficient choice to remove dye contaminants due to its inexpensiveness, simple operation, high efficiency and non-generation of toxic materials (Aichour *et al*., 2019; Jawad and Abdulhameed, 2020). Adsorption is a separation process in which the substances in waste water attach to the inner and outer surfaces of an adsorbent. The adsorbent selectively adsorbs pollutants throughout the separation process, which is due to the specific interaction between the adsorbent surface and the pollutants adsorbed (Crini *et al*., 2019). Therefore, adsorbents

must have mesoporous structures that can be penetrated only by specific molecules, thus producing a molecular sieving effect.

Species are adsorbed on the silica (SiO_2)–alumina (Al_2O_3) surface as this compound, which has a meso- and microporous structure, decomposes, and thus, it also becomes applicable as an eco-friendly and effective adsorbent. Geothermal solid waste is an essential application for dye adsorption resulting in an adequate removal capacity due to its amorphous and mesoporous properties. Amorphous products are extremely important for eliminating MB dye due to their excellent porosity and efficiency (Rożek *et al*., 2019; Siyal *et al*., 2018). Fluid deposition in a geothermal power plant system produces geothermal solid waste that can be used for the synthesis of adsorbent materials as an economical source of silica. The geothermal fluid, which contains a high concentration of dissolved minerals and metals, causes the formation of scales. Silica is frequently found in such a fluid, as it can precipitate unrestrained at various locations in the power plant itself or in the reinjection wells, which cause critical damage to the plant and the reservoir. The geothermal solid waste formed is proportional to the increase in the use of geothermal power as a renewable energy resource, whereas the utilisation of much waste is limited to agricultural and cement materials (Frick *et al*., 2019; Pambudi, 2018; Widayat *et al*., 2020).

A previous study used a mixture of geothermal solid waste and metakaolin as polymer material through a thermal process. The addition of geothermal waste produced a porous material due to its silica content (Gomez-Zamorano *et al*., 2016). The silica–alumina phase has been synthesised from a geothermal solid with a high surface area and molecular sieve characteristics; thus, geothermal waste is very important for adsorption technologies (Alnajjar *et al*., 2019; Munfarida *et al*., 2020; Widayat *et al*., 2019, 2020). To the best of the authors' knowledge, no research has been published on the production of an MB adsorbent from geothermal solid waste. A stirred-tank reactor was utilised to synthesise the adsorbent to produce silica–alumina mixed-phase alumina clusters and pure silica zones. Hence, the main objective of this study is to investigate amorphous adsorbent synthesis from geothermal solid waste. MB adsorption study was carried out and adsorption isotherm models were used to validate experimental data.

Materials and methods

Materials

Geothermal solid waste was obtained from the geothermal power plant of PT. Geo Dipa Energi located in Dieng, Wonosobo, Indonesia. This waste had 64.23% silica based on X-ray fluorescence (XRF) characterisation using a Rigaku Supermini 200 XRF spectrometer. Sodium hydroxide (NaOH; 99%) and aluminium hydroxide ($Al(OH)_3$, 99.63%) were purchased from Sigma-Aldrich, Germany, and used in preparing the adsorbent. Aquadest was provided from the membrane research centre of Center of Research and Services, Diponegoro University. MB was acquired from Sigma-Aldrich, USA, as the adsorbate in this study.

Synthesis of the geoadsorbent

The geothermal solid waste was washed and dried as part of the pretreatment process, before being synthesis as an adsorbent. The waste was then reduced in size by powdering using a pestle and mortar and then sieved with 125 mesh. Next, a stirred-tank reactor was used to mix 1000 g of geothermal solid waste and 418 g of aluminium hydroxide with 4 l of aqueous alkali (sodium hydroxide, 3M). The process went on for 8 h with stirring of the solution at 250 rpm at a temperature of 100°C, resulting in clusters of the silica–alumina mixed phase. The temperature and time were chosen because they were the most frequent and ideal conditions for producing good porous material qualities with a large surface area (Busca, 2014; Sheldon *et al*., 2007). Then, the silica-alumina was cooled down to room temperature for 12 h. The geoadsorbent was then dried in an oven to ensure the removal of water. The final step was to remove impurities and carbon (C) by calcining in a Lindberg/Blue M tube furnace (Asheville, NC, USA) at 550°C for 6 h with nitrogen (N_2) flow.

Characterisation of the geoadsorbent

X-ray diffraction (XRD) analysis was performed to investigate the structure and crystallinity of the geoadsorbent by using a Shimadzu XRD-7000 diffractometer with copper (Cu) Kα radiation as the X-ray source at 30 kV and 30 mA. A Jeol JSM-6510LA scanning electron microscope with an accelerating voltage of 20 kV was used to study the surface morphology of the geoadsorbent. Nitrogen adsorption–desorption was used to investigate the specific surface area by using the Brunauer–Emmett–Teller (BET) method and the pore size distribution by using the Barrett–Joyner–Halenda (BJH) method. Fourier transform infrared spectroscopy (FTIR) analysis was done using a PerkinElmer Spectrum Two infrared (IR) spectrometer to determine the functional group of the adsorbent.

MB adsorption study

Batch experimental MB removal by adsorption technique was determined by adding 0.5 g of the geoadsorbent into Erlenmeyer flasks each containing 100 ml of MB solution with different concentrations (100–200 parts per million (ppm)). The geoadsorbent performance test for MB removal was carried out at room temperature (25°C) to be closest to the industrial context. The solutions were magnetically stirred during the adsorption test for 24 h. The sample was taken to evaluate the MB concentration at 0, 30, 60, 90 and 120 min of the adsorption process. After 24 h (equilibrium condition), the sample was filtered using Whatman filter paper to separate the liquid and the adsorbent and then evaluated the final MB concentration. The MB concentration was evaluated by measuring the absorbance with a Hitachi UH5300 ultraviolet/visible spectrophotometer at a wavelength (λ_{max}) of 665 nm. A calibration curve for MB was performed prior to these observations. The regression equation obtained was $Y = 12.04X + 0.1541$ ($r_2 = 0.975$), where Y and X represent the MB

concentration and the absorbance, respectively. The geoadsorbent performance was evaluated by calculating two parameters, the adsorption capacity at equilibrium (q_e) in milligrams/gram of the adsorbent and the removal percentage (E), using the following equations:

$$q_e\ (\mathrm{mg/g}) = \frac{C_0 - C_e}{m} \times V \quad (1)$$

$$E\ (\%) = \frac{C_0 - C_e}{C_0} \times 100 \quad (2)$$

The initial MB concentration (mg/l) is given by C_0, the MB remaining equilibrium concentration (mg/l) by C_e, the solution volume by V (l) and the adsorbent mass (g) by m.

Adsorption isotherm study

The adsorption isotherm study was carried out by using the Langmuir, Freundlich and Temkin models under equilibrium conditions.

Results

Geoadsorbent characterisation

The surface characteristics of the geoadsorbent, such as specific surface area pore size and volume, affect the MB removal (Siyal *et al*., 2018). In this study, the specific surface area was determined using the BET theory. In contrast, the total pore volume was calculated from the amount of nitrogen adsorbed at a relative pressure of 0.99. The BJH method was used to calculate the pore size distribution. The specific surface area, average pore size and the total pore volume of the geoadsorbent are summarised in Table 1. The pore size diameter of the geoadsorbent is in the range 2–50 nm as seen in Figure 1, classified as a mesoporous structure according to International Union of Pure and Applied Chemistry classification, while the pore volume ranges between 0.03 and 0.23 cm^3/g as summarised in Table 2. Figure 2 presented the type IV adsorption-desoprtion isotherm graph that confirmed the mesoporous structure of geoadsorbent (Králik, 2014). The adsorbent pore size is significant to the MB adsorption capacity because MB is a large molecule and mesoporous adsorbents show much higher MB adsorption capacity than microporous adsorbents (Chueachot *et al*., 2018; Nguyen *et al*., 2016; Siyal *et al*., 2018). The average molecular size of MB is 1.43 × 0.61 × 0.4 nm, depending on the

Table 1. Specific surface area and pore size and volume of the geoadsorbent

Specific surface area: m^2/g	Average pore size: nm	Total pore volume: cm^3/g
276.48	22.73	0.27

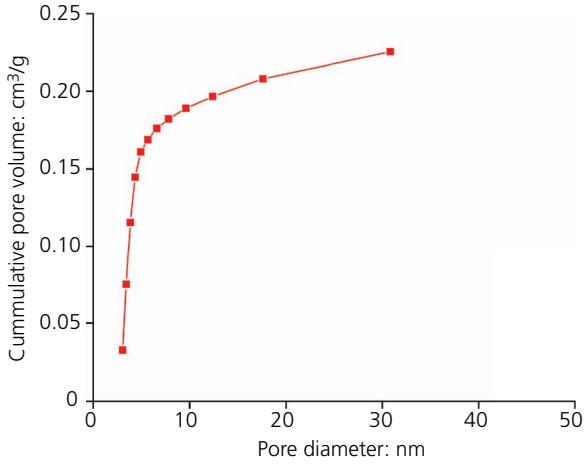

Figure 1. Pore distribution curve

Table 2. Pore size distribution

Pore diameter: nm	Cumulative pore volume: cm^3/g
3.06	0.03
3.42	0.07
3.84	0.12
4.32	0.14
4.91	0.16
5.64	0.17
6.57	0.18
7.79	0.18
9.58	0.19
12.36	0.20
17.55	0.21
30.88	0.23

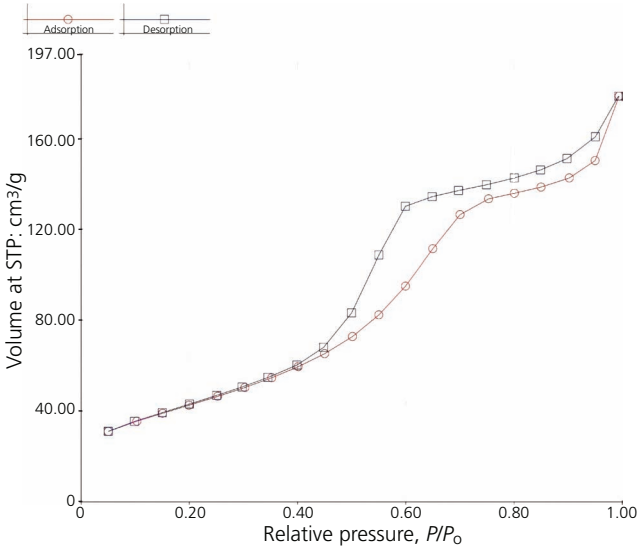

Figure 2. Nitrogen adsorption–desorption of the geoadsorbent. STP, standard temperature and pressure

location of the chloride ion attached to the intermediate sulfur located in the middle of the molecule or one of the two nitrogen atoms located at the edges (Dotto *et al*., 2015; Jia *et al*., 2018; Li *et al*., 2020). Therefore, the molecular size of MB and the surface properties of the geoadsorbent are considered to provide good adsorption capability.

XRD analysis was carried out to identify the zeolite catalyst phase and crystallinity shown through the diffraction peaks. The geoadsorbent diffractogram is presented in Figure 3. The broad and low-intensity peaks that appear indicate that the geoadsorbent is an amorphous material with calculated crystallinity of only 28.16%. The amorphous structure is essential for removing MB due to the formation of a more porous structure, increasing the adsorption capacity (Al-Harahsheh *et al*., 2015; Kara *et al*., 2018). The highest peak intensity of the zeolite catalyst was observed at 2θ of 67.346°/46.0273°/37.6621°. Based on the analysis using the Match software, the peaks show characteristics of natrolite ($Na_2[Al_2Si_3O_{10}]\cdot 2H_2O$). Natrolite crystals were indexed as having an orthorhombic structure (space group: *Fdd*2), with lattice constants a = 17.6780 Å, b = 18.5090 Å and c = 6.4880 Å and a density of 2.214 g/cm^3. The natrolite framework is arranged into T_5O_{10} tetrahedral units (T = Si, Al), whereas natrolite has a SiO_4 tetrahedron as a centre polyhedron surrounded by two SiO_4 and two AlO_4 tetrahedra (Lee *et al*., 2012). The natrolite phase indicates that the silica contained in the geothermal solid waste successfully reacted with aluminium hydroxide and sodium hydroxide. Natrolite has a high specific surface area and adsorptive affinity for organic ions suitable for MB adsorption (Noroozifar *et al*., 2014). The presence of negative charges on aluminium tetrahedra is another important characteristic that generates an increase in MB removal because of electrostatic attraction between positively charged MB and the negatively charged adsorbent (Pathania *et al*., 2017; Rożek *et al*., 2019).

FTIR spectra were obtained in the wave number range from 4000 to 400 cm^{-1} to identify the functional groups on the surface of the geoadsorbent and elucidate the adsorption mechanism. The FTIR spectra of the geoadsorbent before and after MB adsorption are shown in Figure 4. The absorption band of –O (T = Si, Al) bending and Si–O and Al–O tetrahedral vibration at 466 cm^{-1} in the IR spectrum of the geoadsorbent was observed at around 500 cm^{-1} after MB adsorption. The peaks at 800 cm^{-1} show symmetric and asymmetric stretching vibrations, which correspond to the SiO_4 or AlO_4 structure shifting to 844 cm^{-1} with a higher intensity due to the C–C bending of MB. IR bands of the O–Si–O asymmetric stretching of silicon compounds within the wave number range 1130–1000 cm^{-1} were detected in all spectra. The bending vibration of coordinated water is responsible for the peak at 1635 cm^{-1}.

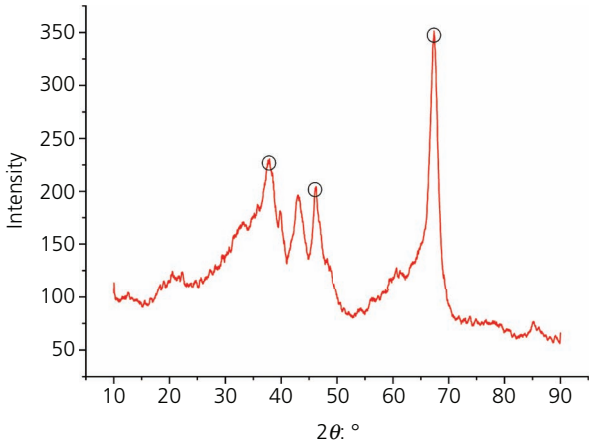

Figure 3. X-ray diffractogram of the geoadsorbent

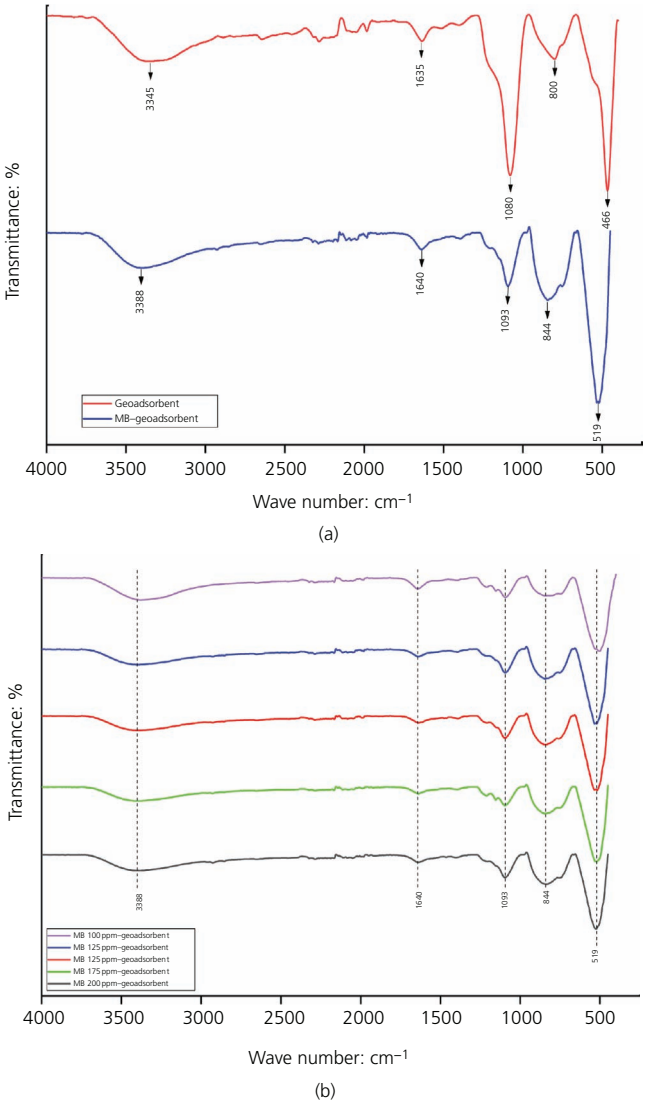

Figure 4. FTIR spectra of the geoadsorbent (a) before and (b) after adsorption of MB

In contrast, the peak of MB–geoadsorbent in the region of 1700–1640 cm^{-1} in the spectrum reflects the $C_{het}=N^{+}(CH_3)_2$ stretching vibrations of MB. The broad absorption peak between 3200 and 3700 cm^{-1} is ascribed to the O–H stretching of the silanol group (Si–OH) and physisorbed water. The peak around 3388 cm^{-1} after MB adsorption caused by O–H stretching vibration broadened due to the hydrogen-bond formation from the $–CH_2$ of MB and MB was adsorbed to the geoadsorbent. The mechanisms of MB adsorption suggest an electrostatic attraction between carboxylic groups and MB cations as well as hydrogen bonds between OH groups on the adsorbent surface and the carbon atoms (Abdelrahman *et al*., 2019; Khanday *et al*., 2017; Li *et al*., 2020; Ovchinnikov *et al*., 2016; Pal *et al*., 2013; Pérez-Morales *et al*., 2019). After MB adsorption, the IR spectrum of the geoadsorbent displays the same bands with some modest shifting, indicating that the functional groups of the geoadsorbent were involved in the MB dye adsorption without any reaction (Jawad and Abdulhameed, 2020).

Scanning electron microscopy (SEM) was used to investigate the surface structure and morphology of the geoadsorbents. SEM images of the geoadsorbent and MB–geoadsorbent (geoadsorbent with adsorbed MB) are presented in Figure 5. Figure 5(a) shows a morphological image of the geoadsorbent at a magnification of ×10 000, which has a roughly pentagonal structure. The rough surface of the geoadsorbent gives a larger surface area for the adsorption of dye contaminants because of its molecular diffusion ability (Aichour *et al*., 2019). As shown in Figures 5(b)–5(f), small irregularly shaped particles covered almost the entire surface of the MB–geoadsorbents. This study demonstrated that MB adsorption changes the surface morphology of geoadsorbents (Li *et al*., 2020).

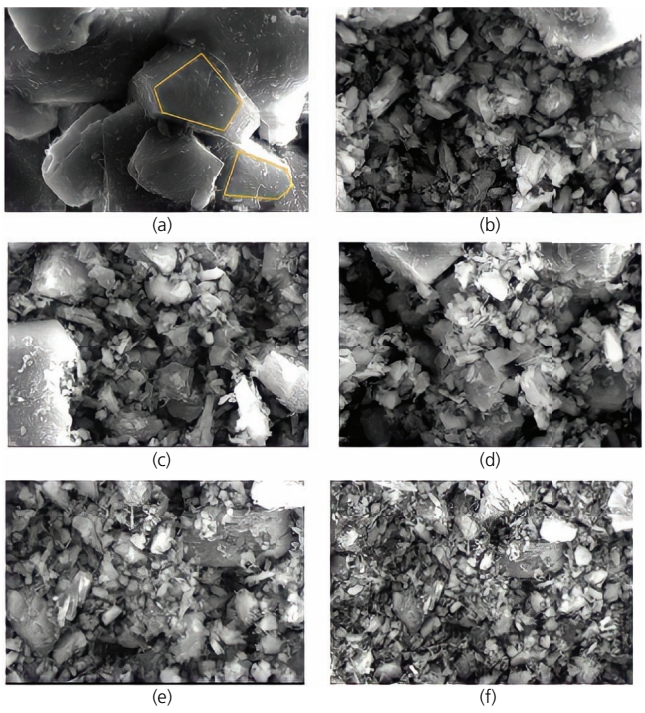

Figure 5. SEM images of (a) the geoadsorbent, (b) 100 ppm MB–geoadsorbent, (c) 125 ppm MB–geoadsorbent, (d) 150 ppm MB–geoadsorbent, (e) 175 ppm MB–geoadsorbent and (f) 200 ppm MB–geoadsorbent

Adsorption study of the geoadsorbent

MB adsorption was studied at various time intervals with initial concentrations of 100–200 mg/l with an adsorbent dose of 0.5 g/l at 25°C. From Figure 6, the MB adsorbed increased rapidly in the first 30 min, becoming slow after that and reaching equilibrium at 210 min at a concentration of 100 mg/l, 240 min at the higher concentrations (125–175 mg/l) and 270 min at 200 mg/l. The initial concentration determines the attainment of equilibrium, where it was possible to identify that the kinetics becomes slower as the concentration increases. There was no significant change in the percentage of dye removal with time after attaining the equilibrium condition. The rate of adsorbate removal from aqueous solutions is primarily controlled by the transfer of dye molecules from the surrounding sites to adsorbent particles (Banerjee and Chattopadhyaya, 2017; Rosset *et al*., 2020).

A decrease in the number of vacant adsorbent sites causes a decrease in MB uptake before 180 min, where initially the ratio between vacant adsorbent sites and MB molecules was very high. The fluctuating change in MB removal shows that physisorption occurred as shown by the reversible removal process, as the MB molecule could be adsorbed and desorbed before the equilibrium condition (Chen *et al*., 2021).

It was found in Figure 7 that the adsorption capacity at equilibrium increased (q_e) from 16.899 to 22.849 mg/g as the

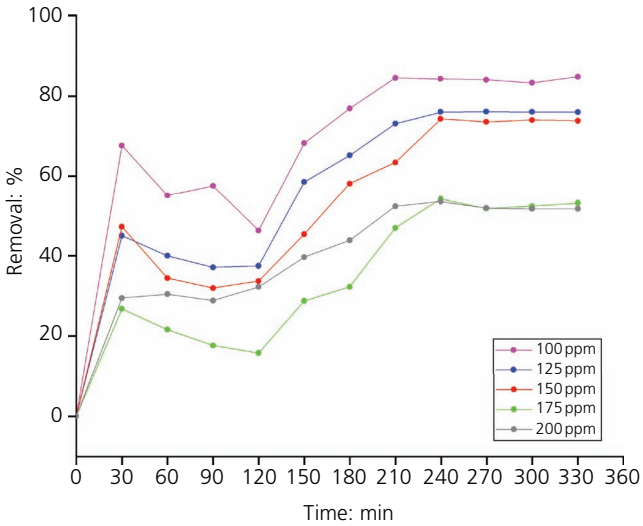

Figure 6. Removal percentage (E) by the geoadsorbent at different initial MB concentrations

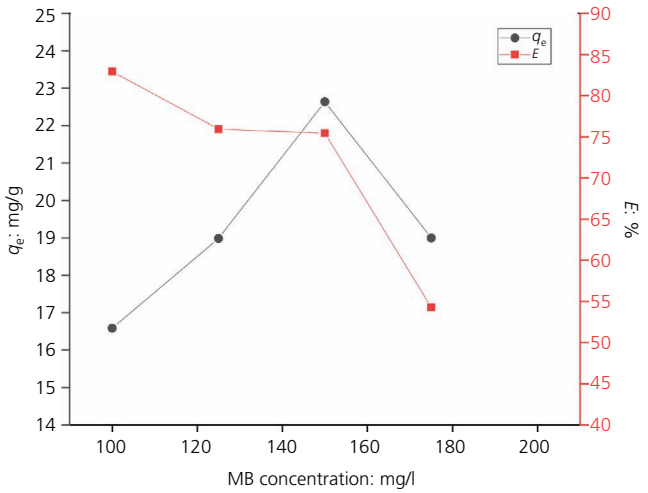

Figure 7. Maximum MB removal percentage (E) and adsorption capacity at equilibrium (q_e)

initial concentration increased from 100 to 150 ppm and the removal percentage decreased with the increase in initial MB concentration in this study. The maximum adsorption capacity at equilibrium is 84.494% at 150 ppm. In comparison, MB concentration of more than 150 ppm led to a decreasing MB adsorbed amount. This means that the adsorption highly depends on the initial concentration of MB. The decrease in adsorption capacity that occurs as a result of increasing concentrations raises the probability that MB monolayers may be forming on the surface of the adsorbent. Lower concentrations provide high efficiency of MB molecule adsorption since fewer available adsorption sites for higher concentrations MB uptake are affected due to the high ratio of the adsorbent surface area to the total MB molecules (Khodaie *et al.*, 2013; Kuang *et al.*, 2020; Pathania *et al.*, 2017).

Isotherm study of MB adsorption

In this work, the adsorption isotherms show an interaction between MB molecules and the geoadsorbent. Many isotherm models can accommodate the correlation between q_e and C_e. The experimental data were fitted to the Langmuir, Freundlich and Temkin isotherm models to study the adsorption isotherms. The adsorption isotherms were obtained from different MB concentrations, where the adsorption capacity needs to be found in equilibrium.

The Langmuir isotherm explains the homogeneous nature of MB adsorption. This occurrence meant that all sites had been saturated, as there was no longer any contact with adsorbent molecules. In its formulation, the empirical model of the Langmuir isotherm assumes monolayer adsorption onto a surface with a finite number of well-defined local sites (Rehman *et al.*, 2021; Wang *et al.*, 2018). The linearised Langmuir model is written mathematically as

$$3.\quad \frac{C_e}{q_e} = \frac{C_e}{q_m} + \frac{1}{K_L q_m}$$

where C_e is the equilibrium concentration of the adsorbate (mg/l), q_e is the amount adsorbed (adsorbate) at equilibrium per unit mass of the adsorbent (mg/g), K_L is the Langmuir constant related to adsorption capacity (l/mg) and q_m is the practical limiting adsorption capacity (mg/g).

Figure 8(a) shows that the Langmuir isotherm model in this study obtained $q_m = 21.673$ as calculated from the slope and $K_L = 0.310$ from the intercept of the plot.

The Freundlich isotherm defines the non-ideal reversible adsorption process that occurs on heterogeneous surfaces and pertains to adsorption processes that occur on heterogeneous surfaces (Rehman *et al.*, 2021; Wang *et al.*, 2018). Mathematically, the linear form of the Freundlich isotherm model can be written as the following equation:

$$4.\quad \log q_e = K_F + \frac{1}{n}\log C_e$$

where C_e is the equilibrium concentration of the adsorbate (mg/l), q_e is the amount adsorbed (adsorbate) at equilibrium per unit mass of the adsorbent (mg/g), K_F is the Freundlich constant related to adsorption capacity (l/mg) and n is the surface heterogeneity or adsorption intensity factor (mg/g).

The Freundlich isotherm plot in this study resulted in a value of $n = 9.163$ calculated from the slope, and $K_F = 13.170$ from the intercept as can be seen in Figure 8(b).

By neglecting deficient and high concentrations, the Temkin isotherm model explains the influence of indirect adsorbate–adsorbent interactions on the adsorption process. This model implies that as the surface coverage of the layer increases, the heat of adsorption of all molecules in the layer decreases linearly (Rehman *et al.*, 2021; Wang *et al.*, 2018). The linearised Temkin isotherm model can be written as in the equation

$$5.\quad q_e = \frac{RT}{b}\ln K_T + \frac{RT}{b}\ln C_e$$

where C_e is the equilibrium concentration of the adsorbate (mg/l), q_e is the amount adsorbed (adsorbate) at equilibrium per unit mass of the adsorbent (mg/g), K_T is the Temkin isotherm constant (l/g), R is the universal gas constant (J/(mol K)), T is the absolute temperature (K) and b is the Temkin constant that is related to heat (J/mol).

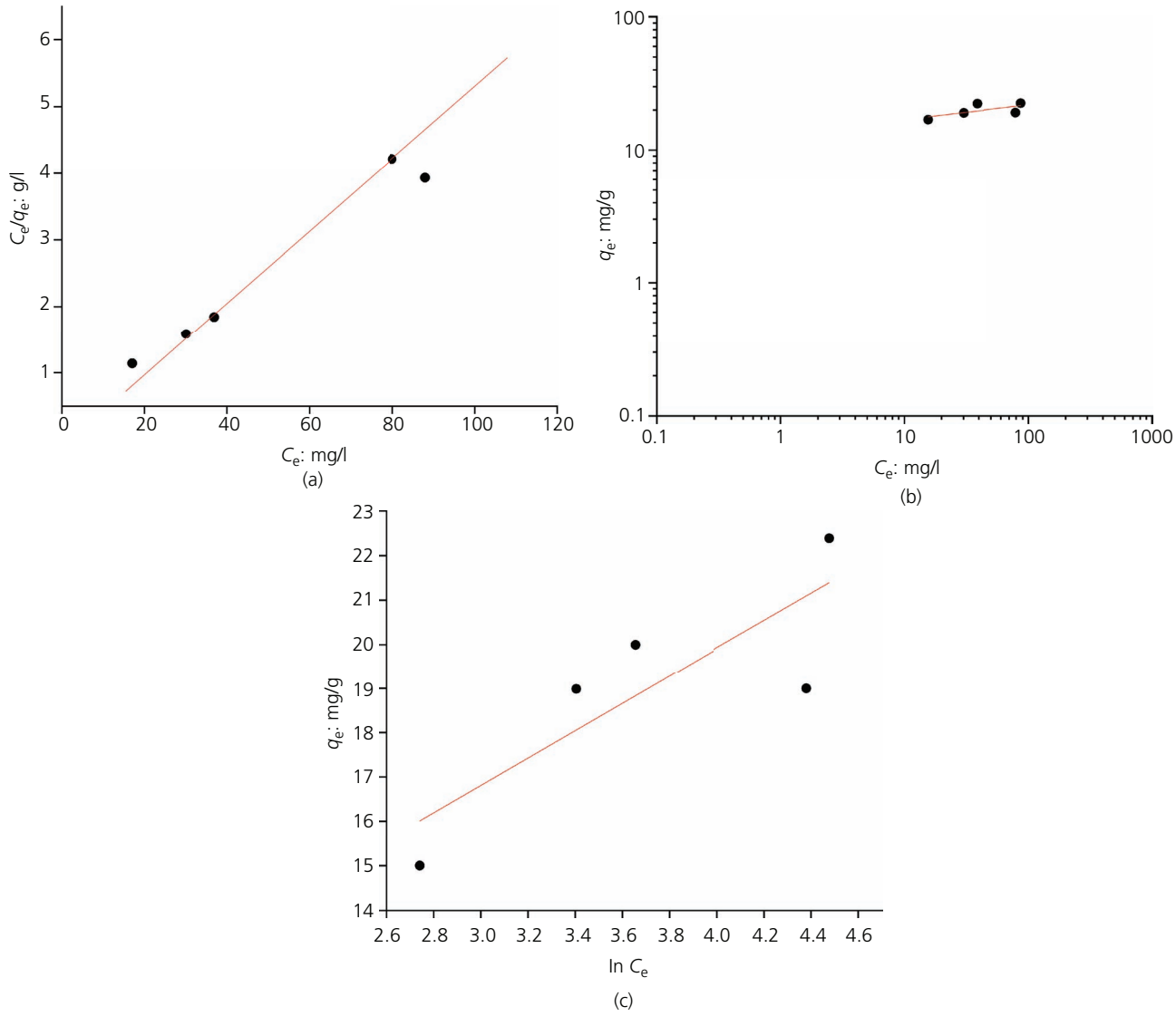

Figure 8. MB adsorption isotherms using the (a) Langmuir, (b) Freundlich and (c) Temkin models

The values of b and K_T were respectively 801.282 and 1.407 × 10^6, calculated from the slope and intercept of the plot q_e against ln C_e shown in Figure 8(c).

Table 3 summarises the parameters of various isotherm models for MB adsorption by the geoadsorbent. It was observed that the Langmuir adsorption isotherm model provided the best fit, with a correlation coefficient of 0.971 being obtained. This suggests that in this study, MB adsorption by the geoadsorbent can be described more accurately by the Langmuir model than by any of the other isotherm models. This is appropriate to the MB monolayer formation caused by adsorption at certain homogeneous locations within the adsorbent (Khodaie *et al.*, 2013).

Conclusions

An amorphous mesoporous geoadsorbent was successfully synthesised for MB removal from geothermal solid waste. The peak diffractogram of the geoadsorbent exhibited an amorphous

Table 3. Isotherm model parameters

T: K	Langmuir			Freundlich			Temkin		
	K_L	q_m	R^2	K_F	n	R^2	K_T	b	R^2
298	0.3104	21.673	0.971	13.17	9.1625	0.4308	1 407 784.8	801.28	0.5974

phase of natrolite, an important characteristic for MB uptake. Equilibrium data fitted well the Langmuir isotherm models rather than the Freundlich and Temkin ones, indicating a homogeneous adsorption process. The capacity of MB removal by the geoadsorbent was up to 84.494% at a concentration of 100 mg/l. Hydrogen bonds between OH groups on the adsorbent surface and electrostatic interaction between carboxylic groups and MB cations governed the dye removal. From this study, it can be concluded that geothermal solid waste offers promise as an effective and sustainable adsorbent for MB removal. This work can be extended to optimise the adsorbent synthesis process and the effect of adsorption operating conditions (pH, temperature, adsorbent dosage).

Acknowledgement

The authors would like to acknowledge the Penelitian Pendidikan Magister Menuju Doktor Untuk Sarjana Unggulan scheme (grant SPK 642-10/UN7.6.1/PP/2020), the Ministry of Research, Technology and Higher Education of the Republic of Indonesia, which funded this project.

REFERENCES

Abdelrahman EA, Hegazey RM and El-Azabawy RE (2019) Efficient removal of methylene blue dye from aqueous media using Fe/Si, Cr/Si, Ni/Si, and Zn/Si amorphous novel adsorbents. *Journal of Materials Research and Technology* **8(6)**: 5301–5313, https://doi.org/10.1016/j.jmrt.2019.08.051.

Aichour A, Zaghouane-Boudiaf H, Zuki FBM, Aroua MK and Ibbora CV (2019) Low-cost, biodegradable and highly effective adsorbents for batch and column fixed bed adsorption processes of methylene blue. *Journal of Environmental Chemical Engineering* **7(5)**: article 103409, https://doi.org/10.1016/j.jece.2019.103409.

Al-Harahsheh MS, Al Zboon K, Al-Makhadmeh L, Hararah M and Mahasneh M (2015) Fly ash based geopolymer for heavy metal removal: a case study on copper removal. *Journal of Environmental Chemical Engineering* **3(3)**: 1669–1677, https://doi.org/10.1016/j.jece.2015.06.005.

Alnajjar M, Hethnawi A, Nafie G *et al.* (2019) Silica–alumina composite as an effective adsorbent for the removal of metformin from water. *Journal of Environmental Chemical Engineering* **7(3)**: 1–10, https://doi.org/10.1016/j.jece.2019.102994.

Banerjee S and Chattopadhyaya MC (2017) Adsorption characteristics for the removal of a toxic dye, tartrazine from aqueous solutions by a low cost agricultural by-product. *Arabian Journal of Chemistry* **10**: S1629–S1638, https://doi.org/10.1016/j.arabjc.2013.06.005.

Busca G (2014) Zeolites and other structurally microporous solids as acid–base materials. In *Heterogeneous Catalytic Materials: Solid State Chemistry, Surface Chemistry and Catalytic Behaviour*. Elsevier, Amsterdam, the Netherlands, pp. 197–249.

Chen Q, Zhang Q, Yang Y *et al.* (2021) Synergetic effect on methylene blue adsorption to biochar with gentian violet in dyeing and printing wastewater under competitive adsorption mechanism. *Case Studies in Thermal Engineering* **26**: article 101099, https://doi.org/10.1016/j.csite.2021.101099.

Chueachot R, Wongkhueng S, Khankam K *et al.* (2018) Adsorption efficiency of methylene blue from aqueous solution with amine-functionalized mesoporous silica nanospheres by co-condensation biphasic synthesis: adsorption condition and equilibrium studie. *Materials Today: Proceedings* **5(6)**: 14079–14085, https://doi.org/10.1016/j.matpr.2018.02.066.

Crini G, Lichtfouse E, Wilson LD and Morin-Crini N (2019) Conventional and non-conventional adsorbents for wastewater treatment. *Environmental Chemistry Letters* **17**: 195–213, https://doi.org/10.1007/s10311-018-0786-8.

Dotto GL, Santosa JMN, Rodriguesa LL *et al.* (2015) Adsorption of methylene blue by ultrasonic surface modified chitin. *Journal of Colloid and Interface Science* **446**: 133–140, https://doi.org/10.1016/j.jcis.2015.01.046.

Frick S, Kranz S, Kupfermann G, Saadat A and Huenges E (2019) Making use of geothermal brine in Indonesia: binary demonstration power plant Lahendong/Pangolombian. *Geothermal Energy* **7(1)**: article 30, https://doi.org/10.1186/s40517-019-0147-2.

Gomez-Zamorano LY, Vega-Cordero E and Struble L (2016) Composite geopolymers of metakaolin and geothermal nanosilica waste. *Construction and Building Materials* **115**: 269–276, https://doi.org/10.1016/j.conbuildmat.2016.03.002.

Jalali K, Pajootan E and Bahrami H (2019) Elimination of hazardous methylene blue from contaminated solutions by electrochemically magnetized graphene oxide as a recyclable adsorbent. *Advanced Powder Technology* **30(10)**: 2352–2362, https://doi.org/10.1016/j.apt.2019.07.018.

Jawad AH and Abdulhameed AS (2020) Mesoporous Iraqi red kaolin clay as an efficient adsorbent for methylene blue dye: adsorption kinetic, isotherm and mechanism study. *Surfaces and Interfaces* **18**: article 100422, https://doi.org/10.1016/j.surfin.2019.100422.

Jia P, Tan H, Liu K and Gao W (2018) Removal of methylene blue from aqueous solution by bone char. *Applied Sciences* **8(10)**: article 1903, https://doi.org/10.3390/app8101903.

Kara I, Tunc D, Sayin F and Akar ST (2018) Study on the performance of metakaolin based geopolymer for Mn(II) and Co(II) removal. *Applied Clay Science* **161**: 184–193, https://doi.org/10.1016/j.clay.2018.04.027.

Khanday WA, Marrakchi F, Asif M and Hameed BH (2017) Mesoporous zeolite–activated carbon composite from oil palm ash as an effective adsorbent for methylene blue. *Journal of the Taiwan Institute of Chemical Engineers* **70**: 32–41, https://doi.org/10.1016/j.jtice.2016.10.029.

Khodaie M, Ghasemi N, Moradi B and Rahimi M (2013) Removal of methylene blue from wastewater by adsorption onto $ZnCl_2$ activated corn husk carbon equilibrium studies. *Journal of Chemistry* **2013**: article 383985, https://doi.org/10.1155/2013/383985.

Králik M (2014) Adsorption, chemisorption, and catalysis. *Chemical Papers* **68(12)**: 1625–1638, https://doi.org/10.2478/s11696-014-0624-9.

Kuang Y, Zhang X and Zhou S (2020) Adsorption of methylene blue in water onto activated carbon by surfactant modification. *Water* **12(2)**: article 587https://doi.org/10.3390/w12020587.

Lee Y, Kao CC and Vogt T (2012) Thermal expansion of the superhydrated small-pore zeolite natrolite. *Journal of Physical Chemistry C* **116(5)**: 3286–3291, https://doi.org/10.1021/jp209514q.

Lellis B, Fávaro-Polonio CZ, Pamphile JA and Polonio JC (2019) Effects of textile dyes on health and the environment and bioremediation potential of living organisms. *Biotechnology Research and Innovation* **3(2)**: 275–290, https://doi.org/10.1016/j.biori.2019.09.001.

Li H, Liu L, Cui J *et al.* (2020) High-efficiency adsorption and regeneration of methylene blue and aniline onto activated carbon from waste edible fungus residue and its possible mechanism. *RSC Advances* **10(24)**: 14262–14273, https://doi.org/10.1039/d0ra01245a.

Mahamad MN, Zaini MAA and Zakaria ZA (2015) Preparation and characterization of activated carbon from pineapple waste biomass for dye removal. *International Biodeterioration and Biodegradation* **102**: 274–280, https://doi.org/10.1016/j.ibiod.2015.03.009.

Munfarida S, Widayat, Satriadi H *et al.* (2020) Geothermal industry waste-derived catalyst for enhanced biohydrogen production. *Chemosphere* **258**: article 127274, https://doi.org/10.1016/j.chemosphere.2020.127274.

Nakhli A, Bergaoui M, Toumi KH *et al.* (2020) Molecular insights through computational modeling of methylene blue adsorption onto low-cost adsorbents derived from natural materials: a multi-model's approach. *Computers and Chemical Engineering* **140**: article 106965, https://doi.org/10.1016/j.compchemeng.2020.106965.

Nguyen NT, Chen S-S, Nguyen NC *et al.* (2016) Adsorption of methyl blue on mesoporous materials using rice husk ash as silica source. *Journal of Nanoscience and Nanotechnology* **16(4)**: 4108–4114, https://doi.org/10.1166/jnn.2016.10704.

Noroozifar M, Khorasani-Motlagh M and Naderpour H (2014) Modified nanocrystalline natural zeolite for adsorption of arsenate from wastewater: isotherm and kinetic studies. *Microporous and Mesoporous Materials* **197**: 101–108, https://doi.org/10.1016/j.micromeso.2014.05.037.

Ovchinnikov OV, Evtukhova AV, Kondratenko TS *et al.* (2016) Manifestation of intermolecular interactions in FTIR spectra of methylene blue molecules. *Vibrational Spectroscopy* **86**: 181–189, https://doi.org/10.1016/j.vibspec.2016.06.016.

Pal P, Das JK, Das N and Bandyopadhyay S (2013) Synthesis of NaP zeolite at room temperature and short crystallization time by sonochemical method. *Ultrasonics Sonochemistry* **20(1)**: 314–321, https://doi.org/10.1016/j.ultsonch.2012.07.012.

Pambudi NA (2018) Geothermal power generation in Indonesia, a country within the ring of fire: current status, future development and policy. *Renewable and Sustainable Energy Reviews* **81**: 2893–2901, https://doi.org/10.1016/j.rser.2017.06.096.

Pathania D, Sharma S and Singh P (2017) Removal of methylene blue by adsorption onto activated carbon developed from *Ficus carica* bast. *Arabian Journal of Chemistry* **10**: S1445–S1451, https://doi.org/10.1016/j.arabjc.2013.04.021.

Pérez-Morales JM, Sánchez-Galván G and Olguín EJ (2019) Continuous dye adsorption and desorption on an invasive macrophyte (*Salvinia minima*). *Environmental Science and Pollution Research* **26(6)**: 5955–5970, https://doi.org/10.1007/s11356-018-04097-8.

Rehman K, Shahzad T, Sahar A *et al.* (2018) Effect of Reactive Black 5 azo dye on soil processes related to C and N cycling. *PeerJ* **6**: article e4802, https://doi.org/10.7717/peerj.4802.

Rehman MU, Manan A, Uzair M *et al.* (2021) Physicochemical characterization of Pakistani clay for adsorption of methylene blue: kinetic, isotherm and thermodynamic study. *Materials Chemistry and Physics* **269**: article 124722, https://doi.org/10.1016/j.matchemphys.2021.124722.

Rosset M, Sfreddo LW, Perez-Lopez OW and Féris LA (2020) Effect of concentration in the equilibrium and kinetics of adsorption of acetylsalicylic acid on ZnAl layered double hydroxide. *Journal of Environmental Chemical Engineering* **8(4)**: article 103991, https://doi.org/10.1016/j.jece.2020.103991.

Rożek P, Król M and Mozgawa W (2019) Geopolymer–zeolite composites: a review. *Journal of Cleaner Production* **230**: 557–579, https://doi.org/10.1016/j.jclepro.2019.05.152.

Sheldon RA, Arends IWCE and Hanefeld U (2007) Green chemistry and catalysis. In *Green Chemistry and Catalysis*. Wiley-VCH, Weinheim, Germany, pp. 1–47.

Shindhal T, Rakholiya P, Varjani S *et al.* (2021) A critical review on advances in the practices and perspectives for the treatment of dye industry wastewater. *Bioengineered* **12(1)**: 70–87, https://doi.org/10.1080/21655979.2020.1863034.

Siyal AA, Shamsuddin MR, Khan MI *et al.* (2018) A review on geopolymers as emerging materials for the adsorption of heavy metals and dyes. *Journal of Environmental Management* **224**: 327–339, https://doi.org/10.1016/j.jenvman.2018.07.046.

Wang M, Xie R, Chen Y *et al.* (2018) A novel mesoporous zeolite-activated carbon composite as an effective adsorbent for removal of ammonia-nitrogen and methylene blue from aqueous solution. *Bioresource Technology* **268**: 726–732, https://doi.org/10.1016/j.biortech.2018.08.037.

Widayat, Hadiyanto, Satriadi H *et al.* (2019) Synthesis of zeolite X molecular sieve from geothermal solid waste. *Materials Today: Proceedings* **13(Part 1)**: 137–142, https://doi.org/10.1016/j.matpr.2019.03.203.

Widayat, Philia J, Farsha T and Rifaldi F (2020) Synthesis of zeolite catalyst from geothermal solid waste for crude glycerol dehydration to acrolein. *Key Engineering Materials* **849**: 130–136, https://doi.org/10.4028/www.scientific.net/KEM.849.130.

How can you contribute?

To discuss this paper, please submit up to 500 words to the editor at journals@ice.org.uk. Your contribution will be forwarded to the author(s) for a reply and, if considered appropriate by the editorial board, it will be published as a discussion in a future issue of the journal.